Decoupling of Transport, Charge Storage, and Interfacial Charge Transfer in the Nanocrystalline TiO_2/Electrolyte System by Impedance Methods

Francisco Fabregat-Santiago,*,† Germà Garcia-Belmonte,† Juan Bisquert,*,† Arie Zaban,‡ and P. Salvador§

Departament de Ciències Experimentals, Universitat Jaume I, 12080 Castelló, Spain, Department of Chemistry, Bar-Ilan University, Ramat-Gan 52900, Israel, and Departamento de Matemáticas e Informática, Universitat de les Illes Balears, Palma de Mallorca, Spain

Received: May 21, 2001; In Final Form: September 17, 2001

Processes in the dark of electron transport and recombination in several nanoporous titanium dioxide films have been studied as a function of the applied potential, using the electrochemical impedance technique. Contact and bulk characteristics have been identified, decoupled, and interpreted, applying a transmission line model that identifies the following elements: (i) the capacitance of the interface between the exposed surface of the substrate and the electrolyte, (ii) the electron transport resistance, (iii) the charge-transfer resistance distributed in the TiO_2/electrolyte interface, and (iv) a distributed capacitive element related to charging the porous matrix. The model provides a satisfactory description of the spectra in widely different conditions of conductivity of the TiO_2 phase. The electron conductivity has been determined as a function of applied potential and coincides for the different samples under study. Classical electrochemical frameworks of transport and interfacial charge transfer used in porous electrodes do not explain the obtained parameters completely. A more complete framework is suggested to explain the system on the basis of the following characteristic features: (i) existence of a large density of electron traps, giving rise both to a trap-limited mobility and to an exponentially increasing capacitance, and (ii) band-edge shifts under external polarization potential.

Introduction

Nanostructured TiO_2 electrodes have attracted widespread attention due to some challenging aspects of their photoelectrochemical properties and their application in the dye-sensitized nanocrystalline solar cells (DSSC).[1] The fact that the semiconductor/electrolyte interface extends to the entire film volume constitutes a main factor for the electrochemical behavior and potential interest of nanoporous TiO_2 photoelectrodes and also implies that transport, reaction, and polarization processes occurring throughout the porous structure are coupled in a rather nontrivial manner. Moreover, the electrochemical behavior of the nanoporous TiO_2 electrode in contact with a redox electrolyte varies widely with the applied voltage or the photon irradiation intensity mainly because changes of the electron population in the TiO_2 phase affect important parameters such as the resistivity and reactivity of the porous network.

Electrochemical impedance spectroscopy is an excellent and well-established technique for characterization of electrochemical systems, most notably in those systems that present a number of coupled processes. In the case of nanostructured TiO_2 electrodes, several simultaneous processes contribute to the overall response to a small ac perturbation: (i) the electron transport in the TiO_2, which is influenced by the free carrier density and electron mobility, the latter being probably dependent on the carrier density, as the electron motion is a trap-limited process,[2−7] (ii) the transfer of electrons to redox species in the electrolyte (sometimes termed recombination or back reaction process in the context of DSSC studies), (iii) the charging of the contact of the transparent conducting substrate (TCS) with the electrolyte (provided that the electrolyte penetrates the porous structure up to the substrate), and (iv) the charging of capacitive elements in the high surface area porous structure, including the Helmholtz capacitance in the TiO_2/electrolyte interface and the capacitances related to filling of the conduction band and surface states of the TiO_2 in the porous structure.[8,9]

Here, we report on impedance measurements of nanoporous TiO_2 electrodes in contact with aqueous solution in the dark. Through a wide variation of the dc applied potential, a change of the TiO_2 behavior from highly insulating to metal-like is obtained. Using a previously reported model,[10] we succeeded in decoupling the different processes i−iv. Impedance results are discussed on the basis of several major points: (i) the general validity of the suggested impedance model, (ii) the decoupling of the substrate and porous network contribution to the impedance response, (iii) the role of a possible potential-induced shift of the TiO_2 band edges,[8,11,12] and (iv) the comparison of a simple diffusion−recombination model, outlined in the Appendix, with a preliminary version of a more advanced model that considers the effect of electron trapping on transport and interfacial charge transfer.

Experimental Section

Attention is centered on a type of sample of nanoporous TiO_2 electrode, prepared from nanocrystals with an average diameter of 49 nm (labeled 101d). The films were made by spreading a TiO_2 paste over a transparent conducting substrate (TCS) consisting of F-doped SnO_2 and further sintering in air. Other

* To whom correspondence should be addressed. E-mail for F.F.-S.: fabresan@uji.es. E-mail for J.B.: bisquert@uji.es.
† Universitat Jaume I.
‡ Bar-Ilan University.
§ Universitat de les Illes Balears.

10.1021/jp0119429 CCC: $22.00
Published on Web 12/12/2001

TABLE 1: Main Characteristics of Nanoporous TiO_2 Films under Study

label	colloid average diameter (nm)	film thickness, L (μm)	geometric surface, S_g (cm^2)	approximate porosity, ν (%)
101d	49	3.7	3.3	50
Tk3	11	7.0	1.0	76
Tk5	10	5.0	1.7	70
Tk6	10	8.6	1.0	73

nanoporous TiO_2 electrodes, prepared in a similar way in different laboratories, were also measured to compare the porous network conductivity of all samples. The characteristics and labeling of all samples are summarized in Table 1.

Electrochemical impedance measurements were done in a three-electrode cell, using a standard potentiostat equipped with an impedance spectra analyzer. The amplitude of the ac signal used was 10 mV, and the frequency ranged between 10 kHz and 10 mHz. All potentials are reported against Ag/AgCl, which was used as reference electrode, connected through a saline bridge of 3 M KCl. In experiments with sample 101d, measurements were performed under dc potentials ranging between 1.1 and −0.6 V. The counter electrode was a Pt wire, and the electrolyte consisted of water at pH 2 (0.01 M H_2SO_4). The variation of the parameters with the pH in solution was also investigated and will be reported elsewhere.

Results

Characteristic impedance spectra of the film 101d are represented in Figure 1 as a function of the applied dc potential. All of the spectra can be described by the equivalent circuit shown in Figure 2b, which contains two main components connected in parallel in addition to a series resistance of the bulk electrolyte. The first component, the capacitance Q_{TCS}, relates to the interface between the TCS and the electrolyte. The behavior of this element has been described elsewhere.[13] As it is well-known for electrochemical systems, this element shows some frequency dispersion, which can be described by a constant phase element (CPE). The second component corresponds to the porous TiO_2 network and is represented by a transmission line model previously developed,[10,14−16] according to the expression

$$Z = \left[\frac{R_1 R_3}{1 + (i\omega/\omega_3)^{\beta}}\right]^{1/2} \coth((\omega_3/\omega_L)^{\beta/2}[1 + (i\omega/\omega_3)^{\beta}]^{1/2}) \quad (1)$$

which contains three independent parameters: (i) the electron-transport resistance, R_1 (Ω), (ii) the charge-transfer resistance distributed in the TiO_2/electrolyte interface, R_3 (Ω), and (iii) the distributed capacitive element, Q_3 (F $s^{\beta-1}$), consisting of a constant phase element with exponent β ($Z_3 = Q_3^{-1}(i\omega)^{-\beta}$). These parameters are expressed in eq 1 through the characteristics transport frequency

$$\omega_L = \frac{1}{(R_1 Q_3)^{1/\beta}} \quad (2)$$

and reaction frequency

$$\omega_3 = \frac{1}{(R_3 Q_3)^{1/\beta}} \quad (3)$$

The parameters in eq 1 can be also expressed in terms of local equivalent circuit elements[10] (Figure 2b) by the relationships $R_1 = r_1 L$, $R_3 = r_3/L$, and $Q_3 = q_3 L$, L being the film thickness.

Other contributions to the impedance, such as resistances accounting for charge losses at the TCS/electrolyte interface or hindrances in electron transfer from TiO_2 to TCS, have been observed to be meaningless. In the first case, after direct observation of response from bare TCS at the potentials used, current flow resulted to be negligible in comparison with that from the covered film. In the second, high-frequency modifications expected in impedance spectra, produced by the introduction of a charge-transfer resistance at the TCS/TiO_2 interface, were not observed.

Because the four parameters in the model, Q_{TCS}, R_1, R_3, and Q_3 are sensitive to the applied potential, it is possible to simplify the general model of Figure 2b in certain voltage domains in which the effect of some of them can be neglected. Therefore, at potentials at which the TiO_2 behaves like an insulator, i.e., at potentials positive of that of the conduction band edge, the circuit presented in Figure 2a fits well the experimental data. In our case, this happens at potentials greater than 0.3 V at which, in correspondence to Q_{TCS}, the impedance spectra show a line almost perpendicular to the real axis.

At the more negative potentials, here beyond −0.3 V, at which the TiO_2 network is heavily conducting, the data is well-fitted by the simple circuit of Figure 2c. At these negative potentials, R_1 becomes negligible and the capacitance of the high-surface-area TiO_2 is much larger than that of the TCS. The semicircles measured in this potential region fit the Figure 2c model.

Between 0.3 and −0.3 V, impedance data need to be fitted with the full equivalent circuit of Figure 2b. Between −0.1 and −0.3 V, as the Q_{TCS} contribution misses relevance, the shape of the spectra follows closely the previously reported theory,[10,17] showing the form in the model 4 of ref 10 for the case in which R_3 is larger than R_1 (or, in other words, $\omega_L > \omega_3$). In the intermediary zone, between 0.3 and −0.1 V, as R_1 becomes larger than R_3, the impedance spectrum changes to a deformed arc with a slope that, following model 4 of ref 10, should be approximately 1 at high frequencies (case of $\omega_3 > \omega_L$), but because of the coupling between the transmission line and the capacitance of the TCS, this high frequency behavior is not directly evident in the spectra.

The equivalent circuits presented in Figure 2 were used to fit the experimental data of all of the samples, though intensive studies out of the intermediary region where the full model is applied were only done for sample 101d. It must be emphasized that both circuits in Figure 2a,c are particular cases of that of Figure 2b (in panel a $R_1 \rightarrow \infty$ and in panel c $R_1 \rightarrow 0$ and $Q_{TCS} \ll Q_3$).

Now, we will present the evolution of the parameters obtained from those fits. First of all, Figure 3 represents the Mott−Schottky plot of the capacitance observed in the range of positive dc potentials for sample 101d. The correlation between $1/C^2$ and the applied potential exhibits a linear dependence. As discussed in detail elsewhere,[13] this capacitance is attributed to a depletion layer at the surface of the TCS exposed to the electrolyte. The donor density calculated from the slope of this Mott−Schottky plot is 1.2×10^{21} cm^{-3}, which is in good agreement with the expected values for this TCS.

The fitting values, R_1, R_3, Q_3, and ω_L, which were calculated from eq 2, are represented in Figure 4part a−d, respectively. All of these four parameters show an exponential dependence on the applied potential, which will be discussed in the next section. Meanwhile, we note that all parameters reported in Figure 4 show continuity with the dc potential despite the change of the impedance function form through the various domains

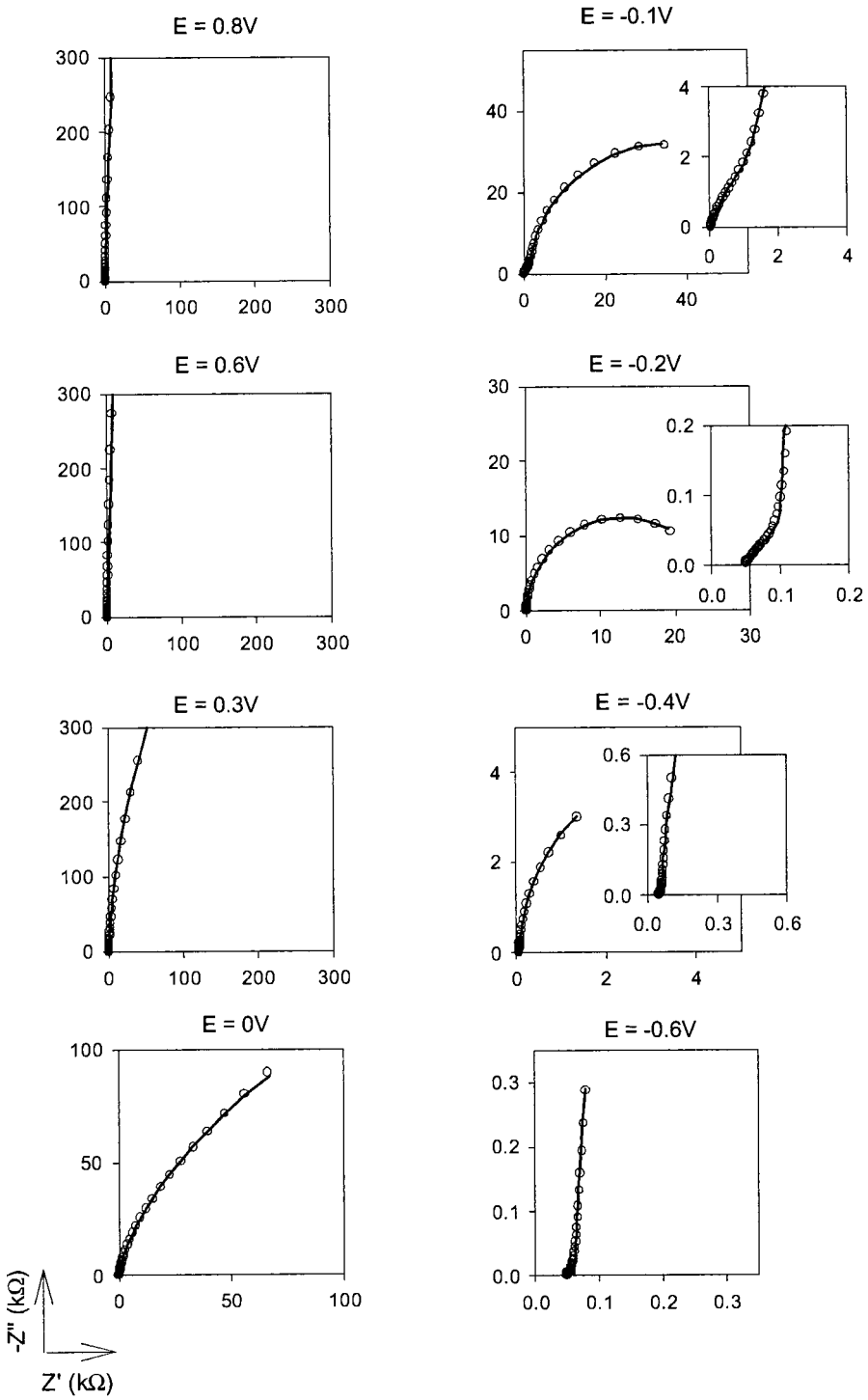

Figure 1. Experimental (○) and fit (—) data of impedance spectra at different applied potentials for sample 101d.

of the potential as commented before. This continuity supports the proposed impedance modeling. β takes values between 0.95 and 0.99, indicating that Q_3 has very low frequency dispersion so it can be considered as an almost ideal capacitor.

The electron conductivities of the porous TiO_2 samples were calculated from the transport resistance according to the expression

$$\sigma_n = \frac{L}{R_1 A(1-\nu)} \tag{4}$$

where ν is the porosity. The calculated conductivities are shown in Figure 5.

Discussion

The experimental results outlined in the previous section show that the impedance model describes well the impedance spectra throughout a wide frequency range for all of the investigated dc potentials. Therefore, it appears that the model presented in Figure 2 provides a rather complete description of the relaxation behavior of the nanoporous TiO_2 electrodes.

A particularly interesting aspect concerns the TCS influence on the overall response of the electrode, something that is not generally acknowledged in similar studies based on the use of frequency-resolved techniques. The TCS effect was discussed in a theoretical study developed on the basis of a general

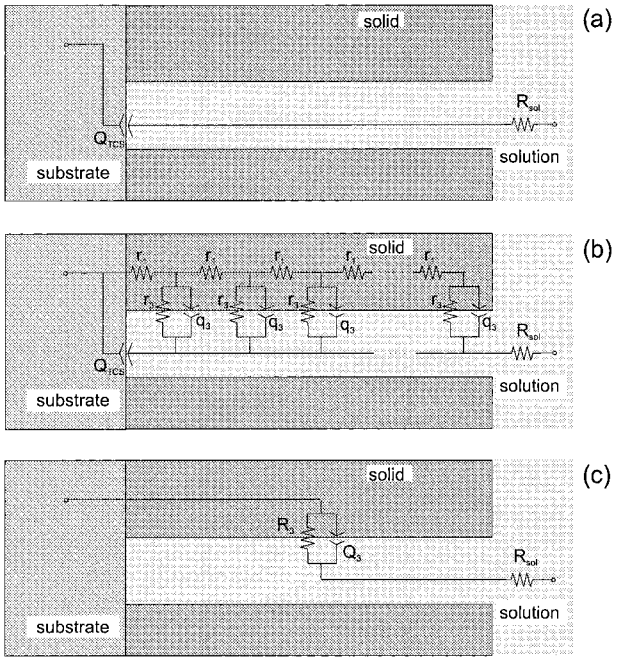

Figure 2. Equivalent circuits used to fit impedance data at the different dc applied potentials. At positive potentials, only the capacitance from the TCS/electrolyte interface, Q_{TCS}, responds to the ac perturbation (a). As the applied potential becomes negative, transport, charge storage, and charge transfer in TiO_2 contribute to the impedance with a transmission line (b). At more negative voltages, the contribution of Q_{TCS} and R_1 to the impedance becomes negligible and the transmission line simplifies to a parallel RC equivalent circuit (c).

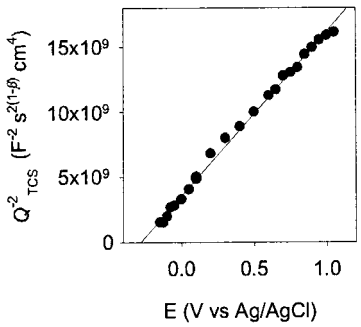

Figure 3. Mott−Schottky plot of the substrate capacitance, Q_{TCS}, for sample 101d.

assessment of the boundaries influence on the impedance of porous electrodes.[15] More specifically, the capacitive response of the TCS as part of a nanoporous TiO_2 electrode has been considered in detail in a separate study, in which the Mott−Schottky behavior of this capacitance is characterized.[13] However, in this second work, the applied potential was restricted to the range in which the TiO_2 network behaves like a dielectric.[13] Here, we apply a more general model for a wider potential range showing that the substrate contribution complies with the linear Mott−Schottky plot even when the TiO_2 exhibits a nonvanishing conductivity. We note as an aside that the distributed impedance model (eq 1 and Figure 2b) that describes the contribution of the porous TiO_2 network has also been used for the analysis of several electrochemical systems with similar characteristics, such as electronically conducting polymers[14,18,19] and porous electrocatalytic IrO_2 electrodes.[20]

To achieve better understanding of the nanoporous system, a further analysis of the physical meaning of the fitting parameters R_1, R_3, and Q_3 seems necessary. We recall that eq 4 implicitly contains the dependence of the electron conductivity, σ_n, on the applied voltage. Because all of the TiO_2 films have

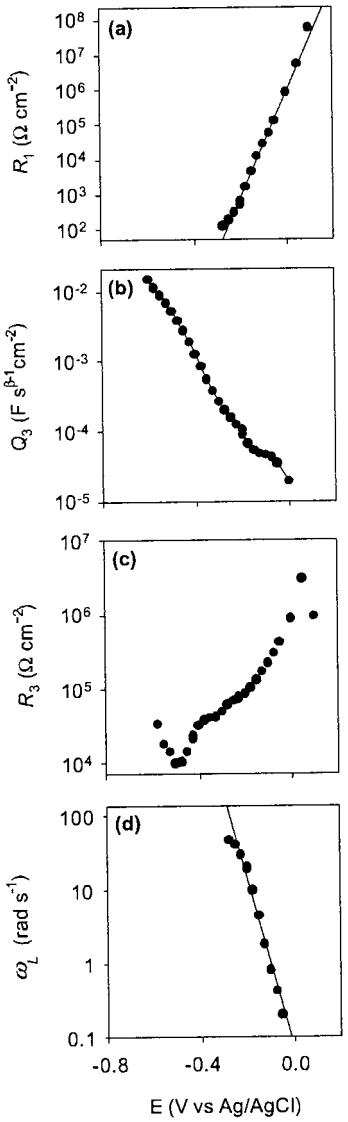

Figure 4. Best fits of parameters R_1 (a), Q_3 (b), R_3 (c) (per projected area), and ω_L (d) for sample 101d.

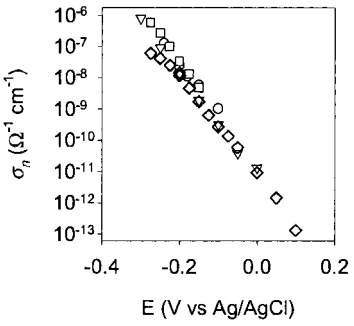

Figure 5. Potential dependence of the electron conductivity for the different samples studied, 101d (◇), Tk3 (○), Tk5 (▽), and Tk6 (□) at pH 2 calculated from R_1 according to eq 4.

a similar configuration, their electron conductivity is expected to be comparable independent of their origin, thickness, and porosity, as is in fact shown in Figure 5.

The electron conductivity depends on the electron mobility, μ_n, and the free electron concentration n as

$$\sigma_n = en\mu_n \tag{5}$$

Moreover, μ_n is related to the diffusion coefficient, D_n, according

to the Einstein relationship

$$\mu_n = \frac{eD_n}{kT} \tag{6}$$

The exponential dependence of R_1 on the applied potential shown in Figure 4a (a slope of 15.5 V^{-1} is obtained) allows an understanding of the dependence of σ_n on the applied voltage. The electron diffusion model, which is widely used to interpret the results of several frequency-resolved techniques,[9,21,22] assumes a constant value for μ_n and D_n, which according to eq 5 implies the entire variation of σ_n should be attributed to changes of free-electron concentration. As shown in another work[16] and summarized in the Appendix, this electron diffusion model leads to the impedance function of eq 1. This model predicts a variation of σ_n of 1 decade per 59 mV, meaning that the slope of R_1 in Figure 4a should be 17 V^{-1} [= 1/59 mV] (see the Appendix), which is higher than the actual experimental value. This discrepancy may be explained on the basis of an upward shift of the TiO_2 band edges as the potential is scanned negatively, as already found by a new technique that measures the correlation of the conductivity to the photovoltage[12] and also by modulated reflectivity measurement,[23] in the dye-sensitized system.

A more complete model for the electron transport in this type of electrode takes into account electron transitions between the extended states of the conduction band and band gap trapping sites in which electrons are temporarily immobilized.[2−6,9,12,22] According to this model, carrier transport is a trap-limited process, and the electron mobility can be described as a concentration-dependent magnitude. In general, a decrease of the trapping time occurs as the quasi-Fermi level approaches the conduction band, because of the increasing occupancy of slower (deeper) band gap states, so an increase of the trap-limited mobility as the potential becomes more negative should be expected, i.e., $\mu_n \propto n^{\epsilon}$ with $\epsilon > 0$, the specific form of ϵ being dependent on the distribution of the traps. According to this argument, we should have $\sigma_n \propto n^{1+\epsilon}$, and if we consider that the band edges are pinned, n increases exponentially with the applied negative voltage as $\exp(-eV/(kT))$ so that the slope in Figure 4a would be larger than 17 V^{-1} (i.e., $(1 + \epsilon)17$ V^{-1}). However, the observed slope is smaller than 17 V^{-1}, which means that the increase of n with the applied voltage is much less rapid than $\exp(-eV/(kT))$. Thus, in this more general approach, it is also necessary to invoke the existence of an upward shift of the band edges as the quasi-Fermi level rises, i.e., a partial Fermi level pinning. Further analysis of the results according to this view requires a more complex ac impedance model, which has not been fully developed yet.

The parameter Q_3 in eq 1 corresponds to a capacitive element distributed through the porous network that is related to the surface charge processes of the TiO_2 network. Because Q_3 increases exponentially with the applied voltage, the capacitance reaches a value of about 10 mF cm^{-2} (per substrate area) at the most negative potentials. This value is of the same order of magnitude as that found in the RuO_2-based electrochemical supercapacitors.[24] The results presented according to our approach in Figure 4b show a slope of 5.3 V^{-1}. This exponential variation of the capacitance with the potential is in agreement with previous reports related to the dye-sensitized system by Zaban et al.[25] and also by van de Lagemaat et al.[26]

In principle, the origin of the exponential increase of the capacitance is also compatible with the simple diffusion model, in which the free-charge capacitance Q_3 (sometimes termed "diffusion capacitance" or "conduction band capacitance") is proportional to the free-electron concentration, n (see eq A5). This interpretation, however, would require an identical slope in log representations of both R_1 and Q_3 vs voltage. In other words, the characteristic frequency, ω_L, of eq 2 should be a constant according to eq A6, which is clearly in contradiction with our results of Figure 4d. It can be concluded therefore that the simple diffusion model does not give a complete description of the system.

Because Q_3 cannot be understood only in terms of the conduction band capacitance, we have to assume that a significant degree of charging occurs by the occupation of surface states by electrons, charge-compensated by protons at the oxyde/water interface.[27,28] In fact, it has been suggested that the effect of electron trapping accounts for the exponential variation of the capacitance.[26] In addition, surface-site charging is a well-established mechanism that explains the large capacitance found in highly porous metal-oxide-based electrochemical supercapacitors.[29]

The characteristic frequency ω_L is related to the transit time through the porous network. The variation of this parameter, reported in Figure 4d, indicates a trap-limited transport mechanism, in which the carrier motion is heavily influenced by the position of the quasi-Fermi level in the energy gap. A dependence of ω_L on the photoexcitation intensity has been found using other types of frequency-resolved techniques.[2,7,30]

In the potential range between −0.3 and +0.2 V (vs Ag/AgCl), i.e., positive of $E°$ (H^+/H_2), the only electrolyte-dissolved species that can be reduced are O_2 molecules;[31] therefore, R_3 must be associated with oxygen reduction. (In fact, it was checked that by bubbling nitrogen gas the R_3 decreases by 2 orders of magnitude.) This parameter, shown in Figure 4c, displays a rather interesting behavior; it decreases up to about −0.5 V and increases at the more negative potentials, at which protons start to be reduced, and R_3 is mainly influenced by H^+ reduction. As we will show elsewhere, this behavior is related to the electron transfer occurring via surface states, which become saturated near flat band.[28,31,32]

In summary, some encouraging results have been found. The measured impedance spectra are quite structured; nevertheless, the basic constituents can be decomposed by the model of Figure 2b, at the different applied voltages, throughout the whole frequency range. This allows one to determine the features of the conductivity as reported in Figure 5, to decouple the substrate charging, and to separate Faradaic and charging components in the transient behavior of the porous network. A detailed analysis of the parameters involved in eq 1 has shown that a simple diffusion−recombination approach[16] provides a simple and useful description of the system though not a completely satisfactory one. It seems necessary to emphasize that, beyond this preliminary approach, the interpretation of some points is not totally clear at the present time. The influence of electron trapping appears significant both in charge storage and in charge transfer in the TiO_2 network. Trapping appears to influence the electron transport as well, judging by the behavior of ω_L; however, the frequency patterns related to dispersive or anomalous electron transport[17,33,19,34] are not detected in the present system. Moreover, surface charging may induce a drift component in the driving force of transport, which is not at all easy to distinguish from the diffusion mechanism on the basis of impedance measurements.[10,16,35] A possible inhomogeneity of the transmission line elements should be considered as well in a more advanced framework. Therefore, for a complete picture of transport, charge transfer, and charge-storage properties of nanoporous TiO_2 to be obtained, an extension of the impedance model will have to be developed and further experimental research is needed.

Conclusions

A transmission line model is compatible with experimental impedance data and allows decoupling of the contributions of both the transparent conducting substrate and the porous TiO_2 film. Several TiO_2 films prepared in different laboratories present a similar conductivity. Coupling between bulk parameters for electron transport (R_1) and charge storage (Q_3) gives place to an exponentially potential-dependent diffusion coefficient. Classical impedance models of porous electrodes that are based on either drift or diffusion mechanisms of electron transport do not explain the results completely. A more advanced framework is needed to explain the results more accurately on the basis of the following features: existence of a large density of electron traps giving rise to a trap-limited mobility with an exponentially increasing capacitance and interfacial charge transfer through the surface states and a shift of the TiO_2 band edges simultaneous with the potentiostatic rise of the quasi-Fermi level, which accounts for the observed potential dependence of R_1.

Acknowledgment. We thank P. Bognanoff of the Hahn-Meitner Institut for supplying some of the samples used in this study. The Fundació Caixa Castelló supported the work.

Appendix: Impedance Analysis of the Simple Electron Diffusion−Recombination Model

This model[21] assumes that the applied voltage, V, lifts the quasi-Fermi level inside the TiO_2, while the conduction band is pinned. Thus, at the TiO_2/SnO_2 contact, the electron concentration increases according to

$$n_s = n_0 \exp(-eV/(kT)) \tag{A1}$$

where n_0 is the equilibrium value in the dark and e and k stand for the positive elementary charge and the Boltzmann constant, respectively. Elsewhere, the electron concentration is determined by the diffusion−recombination equation

$$\frac{\partial n}{\partial t} = D_n \frac{\partial^2 n}{\partial x^2} - \frac{n - n_0}{\tau_r} \tag{A2}$$

where D_n is the electron diffusion coefficient, which is a constant, and τ_r is a kinetic time constant describing the reaction of electrons in the TiO_2 with redox species in the electrolyte. In addition, the edge of the TiO_2 layer at the electrolyte side is a reflecting boundary for electrons.

The impedance of this diffusion−recombination model has been studied separately.[16] It has been shown that the impedance is described by eq 1 for the particular case of $\beta = 1$, in which the parameters take the following form: The transport resistance is

$$R_1 = \frac{kTL}{e^2 A D_n n_s} \tag{A3}$$

Notice that this expression can be written as well

$$R_1 = \frac{L}{A\sigma_s} \tag{A4}$$

where σ_s is the electron conductivity at the TiO_2/SnO_2 contact. The distributed capacitance of eq 1, also termed either diffusion[36,37] or conduction band capacitance,[8,9] takes the form

$$Q_3 = LAe \frac{dn_s}{dV} = \frac{LAe^2 n_s}{kT} \tag{A5}$$

Using eqs 2, A3, and A5, one finds that in this model

$$\omega_L = \frac{D_n}{L^2} \tag{A6}$$

which is a standard result in the theory of diffusion impedance.[37] Finally, the reaction resistance is given by the expression

$$R_3 = \omega_L \tau_r R_1 \tag{A7}$$

References and Notes

(1) O'Regan, B.; Grätzel, M. *Nature* **1991**, *353*, 737.
(2) de Jongh, P. E.; Vanmaekelbergh, D. *Phys. Rev. Lett.* **1996**, *77*, 3427.
(3) Nelson, J. *Phys. Rev. B* **1999**, *59*, 15374.
(4) Könenkamp, R.; Henninger, R. *Appl. Phys. A* **1994**, *58*, 87.
(5) Könenkamp, R. *Phys. Rev. B* **2000**, *61*, 11057.
(6) van de Lagemaat, J.; Frank, A. J. *J. Phys. Chem. B* **2000**, *104*, 4292.
(7) Fisher, A. C.; Peter, L. M.; Ponomarev, E. A.; Walker, A. B.; Wijayantha, K. G. U. *J. Phys. Chem. B* **2000**, *104*, 949.
(8) Schlichthröl, G.; Huang, S. Y.; Sprague, J.; Frank, A. J. *J. Phys. Chem. B* **1997**, *101*, 8141.
(9) Franco, G.; Gehring, J.; Peter, L. M.; Ponomarev, E. A.; Uhlendorf, I. *J. Phys. Chem. B* **1999**, *103*, 692.
(10) Bisquert, J.; Garcia-Belmonte, G.; Fabregat-Santiago, F.; Ferriols, N. S.; Bogdanoff, P.; Pereira, E. C. *J. Phys. Chem. B* **2000**, *104*, 2287.
(11) Cao, F.; Oskam, G.; Meyer, G. J.; Searson, P. C. *J. Phys. Chem.* **1996**, *100*, 17021.
(12) Zaban, A.; Bisquert, J. Unpublished work.
(13) Fabregat-Santiago, F.; Garcia-Belmonte, G.; Bisquert, J.; Zaban, A. submitted for publication.
(14) Bisquert, J.; Garcia-Belmonte, G.; Fabregat-Santiago, F.; Ferriols, N. S.; Yamashita, M.; Pereira, E. C. *Electrochem. Commun.* **2000**, *2*, 601.
(15) Bisquert, J. *Phys. Chem. Chem. Phys.* **2000**, *2*, 4185.
(16) Bisquert, J. *J. Phys. Chem. B* **2002**, *106*, 325.
(17) Bisquert, J.; Garcia-Belmonte, G.; Fabregat-Santiago, F.; Compte, A. *Electrochem. Commun.* **1999**, *1*, 429.
(18) Fletcher, S. *J. Electroanal. Chem.* **1992**, *337*, 127.
(19) Garcia-Belmonte, G.; Bisquert, J.; Pereira, E. C.; Fabregat-Santiago, F. *Appl. Phys. Lett.* **2001**, *78*, 1885.
(20) Terezo, A. J.; Bisquert, J.; Pereira, E. C.; Garcia-Belmonte, G. *J. Electroanal. Chem.* **2001**, *508*, 59.
(21) Södergren, S.; Hagfeldt, A.; Olsson, J.; Lindquist, S. E. *J. Phys. Chem.* **1994**, *98*, 5552.
(22) Dloczik, L.; Ileperuma, O.; Lauerman, I.; Peter, L. M.; Ponomarev, E. A.; Redmond, G.; Shaw, N. J.; Uhlendorf, I. *J. Phys. Chem. B* **1997**, *101*, 10281.
(23) Turrión, M.; Macht, B.; Tributsch, H.; Salvador, P. *J. Phys. Chem. B* **2001**, *105*, 9732.
(24) Conway, B. E. *Electrochemical supercapacitors*; Plenum Publishing: New York, 1999.
(25) Zaban, A.; Meier, A.; Gregg, B. A. *J. Phys. Chem. B* **1997**, *101*, 7985.
(26) van de Lagemaat, J.; Park, N.-G.; Frank, A. J. *J. Phys. Chem. B* **2000**, *104*, 2044.
(27) Boschloo, G.; Fitzmaurice, D. *J. Phys. Chem. B* **1999**, *103*, 7860.
(28) Wang, H.; He, J.; Boschloo, G.; Lindström, H.; Hagfeldt, A.; Lindquist, S. *J. Phys. Chem. B* **2001**, *105*.
(29) Trasatti, S. In *The Electrochemistry of Novel Materials*; Lipkowski, J., Ross, P. N., Eds.; VCH: Weinheim, Germany, 1994; p 207.
(30) de Jongh, P. E.; Vanmaekelbergh, D. *J. Phys. Chem. B* **1997**, *101*, 2716.
(31) Tafalla, D.; Salvador, P. *Ber. Bunsen-Ges. Phys. Chem.* **1987**, *91*, 475.
(32) Salvador, P.; Gutiérrez, C. *J. Electrochem. Soc.* **1984**, *131*, 326.
(33) Bisquert, J.; Compte, A. *J. Electroanal. Chem.* **2001**, *499*, 112.
(34) Garcia-Belmonte, G.; Bisquert, J.; Pereira, E. C.; Fabregat-Santiago, F. *J. Electroanal. Chem.* **2001**, *508*, 48.
(35) Vanmaekelbergh, D.; de Jongh, P. E. *J. Phys. Chem. B* **1999**, *103*, 747.
(36) Tyagi, M. S. *Introduction to Semiconductor Materials and Devices*; John Wiley and Sons: New York, 1991.
(37) Bisquert, J.; Garcia-Belmonte, G.; Fabregat-Santiago, F.; Bueno, P. R. *J. Electroanal. Chem.* **1999**, *475*, 152.